Highly inclined thin illumination enables clear single-molecule imaging in cells

Makio Tokunaga[1–3], Naoko Imamoto[4,5] & Kumiko Sakata-Sogawa[2]

We describe a simple illumination method of fluorescence microscopy for molecular imaging. Illumination by a highly inclined and thin beam increases image intensity and decreases background intensity, yielding a signal/background ratio about eightfold greater than that of epi-illumination. A high ratio yielded clear single-molecule images and three-dimensional images using cultured mammalian cells, enabling one to visualize and quantify molecular dynamics, interactions and kinetics in cells for molecular systems biology.

Much progress in single-molecule techniques has provided a new and direct approach to study molecular mechanisms[1–9] in recent years. Real-time imaging of single fluorescent molecules in aqueous solution was achieved by refining epifluorescence microscopy[4,5] and total internal reflection fluorescence microscopy (TIRF)[4,6]. As TIRF illuminates only surface areas[10], it has been used to visualize single molecules *in vitro*[11]. Furthermore, single-molecule imaging with objective-type TIRF[6] allowed researchers to observe individual molecules on the cell surface[12,13]. However, the application of TIRF is limited to surfaces. To overcome this limitation, here we describe an approach, called highly inclined and laminated optical sheet (HILO) microscopy for single-molecule imaging inside cells.

The main technical challenge of single-molecule fluorescence imaging is increasing the signal/background ratio. We achieved notable success in this by inclining the illumination beam and by minimizing the illumination area. The incident laser beam is highly inclined by a large refraction and is laminated as a thin optical sheet at the specimen side (**Fig. 1a**,**b**). In HILO microscopy, this thin optical sheet is used for illumination. Its thickness dz along the z-direction is roughly $dz = R/\tan\theta$, which is the thickness of the geometrical optics not including the divergence, where R is the diameter of the illuminated area at the specimen plane, and θ is the incidence angle at the specimen (**Fig. 1b**). When $R/\tan\theta$ is less than a few tens of micrometers, divergence increases the thickness dz by more than the value obtained by the calculation above. To reduce the divergence of illumination at the specimen, we incorporated a field stop for the illumination beam into the incident light path to be conjugate with the specimen plane. The image of the field stop is formed at the specimen plane so that the divergence of the illumination at the edge of the field-stop image is minimized (**Fig. 1b** and **Supplementary Fig. 1a**,**b** online).

One of the features of HILO microscopy is that the illumination beam always passes through the center of the specimen plane (**Supplementary Fig. 1c–f**), which means the illumination beam follows the z-directional shift of the specimen plane. This feature is powerful for three-dimensional imaging.

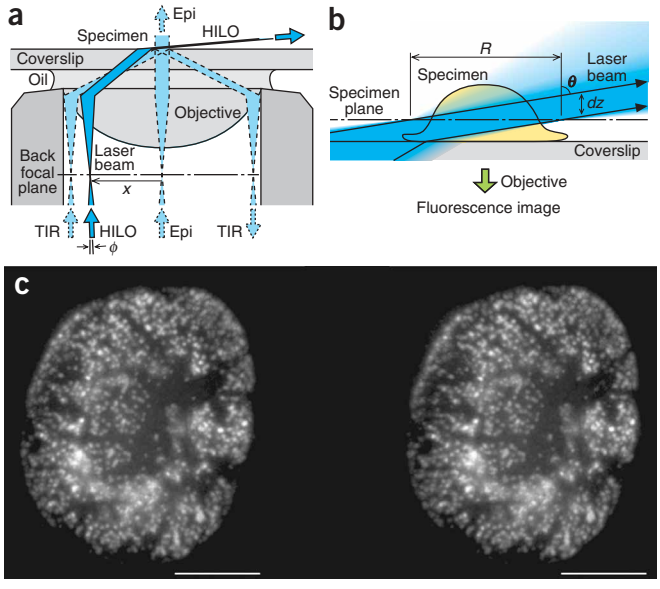

Figure 1 | HILO microscopy for molecular imaging in cells and three-dimensional imaging of the NPCs. (**a**) Optics. The incident beam is positioned to propagate near the objective edge. It is highly inclined by a large refraction at the glass-specimen surface, and then it is laminated as a thin optical sheet on the specimen side. TIR, totally internally reflection fluorescence microscopy for surface imaging; Epi, epifluorescence. (**b**) Specimens are illuminated with a thin sheet of laser beam. (**c**) Stereo pair of a three-dimensional image reconstructed from serial images (see **Supplementary Video 1**). The photobleaching was linearly corrected using to-and-fro scanned images (reduction of image intensity by photobleaching during z-scan from $z = 0$ to 16.2 μm with an interval of 0.44 μm was 11%). The distribution of NPCs on the nuclear envelope is not uniform but often in line, which may indicate a correlation with inner nuclear structures. Scale bars, 5.0 μm.

[1]Biological Macromolecules Laboratory, National Institute of Genetics, Yata 1111, Mishima, Shizuoka 411-8540, Japan. [2]Research Center for Allergy and Immunology, RIKEN, 1-7-22, Suehiro, Tsurumi, Yokohama, Kanagawa 230-0045, Japan. [3]Department of Genetics, School of Life Science, The Graduate University for Advanced Studies, Mishima Shizuoka 411-8540, Japan. [4]Gene Network Laboratory, National Institute of Genetics, Mishima Shizuoka 411-8540, Japan. [5]Cellular Dynamics Laboratory, RIKEN, Wako, Saitama 351-0198, Japan. Correspondence should be addressed to M.T. (mtoku@lab.nig.ac.jp).

RECEIVED 20 AUGUST 2007; ACCEPTED 27 NOVEMBER 2007; PUBLISHED ONLINE 6 JANUARY 2008; DOI:10.1038/NMETH.1171

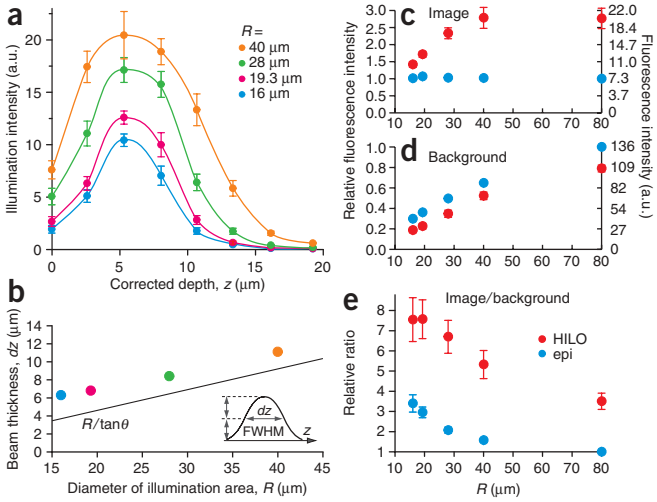

Figure 2 | Thickness of HILO illumination beam and signal/background ratio. (**a**) Profiles of illumination intensity through the *z*-direction at the different illumination diameter *R*. Corrected *z* was calculated from the refractive index of the specimen (**Supplementary Methods**). Error bars indicate s.e.m.; $n = 38$, 36, 38, 38, 40, 33, 42 and 30 microspheres for $z = -0.02$, 2.59, 5.31, 8.04, 10.68, 13.34, 16.14 and 19.24 μm, respectively. (**b**) Full width of half maximum (FWHM) was calculated as the beam thickness *dz* from the profile in **a**. Solid line represents $R/\tan\theta$ according to the geometrical optics ($\theta = 77$ degrees, which is obtained from $x = n \times f_{obj} \times \sin\theta$ and $x/(n \times f_{obj}) = 2.6$ mm/1.334/2 mm; see **Supplementary Fig. 3h**). (**c**–**e**) Comparison of relative fluorescence intensity of microsphere images (**c**) and background (**d**) and signal/background ratio (**e**) between HILO ($x/(n \times f_{obj}) = 2.6$ mm/1.334/2 mm) and epi-illumination. Fluorescent microspheres (diameter of 100 nm) in 1% agar were used, and signal intensity were analyzed as in **Supplementary Figure 4d**. Error bars, s.e.m.; $n = 38$ and 34 microspheres for HILO and epi, respectively (**c**). Error bars, s.d.; $n = 48{,}944$ pixels (**d**). See **Supplementary Methods** for error calculation for **e**.

To evaluate the HILO microscopy technique, we reconstructed three-dimensional images of the nuclear pore complexes (NPCs) in cells from *z*-scanned serial images (**Fig. 1c**, **Supplementary Fig. 2a–c** and **Supplementary Video 1** online). We obtained clear point-like images of NPCs without the need for deconvolution to remove out-of-focus haze (**Fig. 1c**). The fluorescence intensity of the NPCs at the top of the nuclei (14.7 μm above the coverslip surface) was 62% of that at the bottom (**Supplementary Fig. 2d**). The decrease is explained well by the spherical aberration of the objective. Further, there was much lower photobleaching than in conventional confocal microscopy because of the lower intensity and nonfocused nature of illumination.

We examined the thickness *dz* of the illumination beam (**Supplementary Methods** online) and obtained illumination intensity profiles in the *z*-direction (**Fig. 2a**). We decreased the illumination thickness *dz* with the reduction of the illumination diameter *R*, having an additional thickness of a few micrometers derived from divergence to the geometrical optics thickness $R/\tan\theta$ (**Fig. 2b**). Notably, the full width at half maximum of the profile was less than 7 μm at the diameter *R* below 20 μm.

Next we evaluated the signal/background ratio of images in HILO in two ways, using fluorescent microspheres (**Fig. 2c–e**) and using cross-sectional images of the nuclei (**Supplementary Fig. 3** online). Inclination of the illumination beam (larger incidence angle θ, that is, larger incidence distance *x*; **Fig. 1a**) increases intensities of the fluorescence images up to 2.8-fold compared with epi-illumination, that is, $x = 0$ (**Fig. 2c**). Optical theory holds that the intensity of the refracted light increases with θ (that is, *x*; **Supplementary Fig. 3g,h**). Namely, refraction with a larger angle makes the refracted beam thinner, that is, increases the light density. The 2.8-fold increase is in excellent agreement with the theory.

In contrast, the background intensity is substantially decreased by illumination inclination (**Supplementary Fig. 3b**). As the background is composed of out-of-focus images, the decrease is explained by the reduction of the illuminated range. As a result, illumination inclination increased the ratio of image to background (signal/background) up to 3.1–3.5-fold (**Fig. 2e** and **Supplementary Fig. 3c**). Reduction of the illumination diameter *R* further decreased the background intensity (**Fig. 2d** and **Supplementary Fig. 3e**). Consequently, reduction of the diameter *R* increased

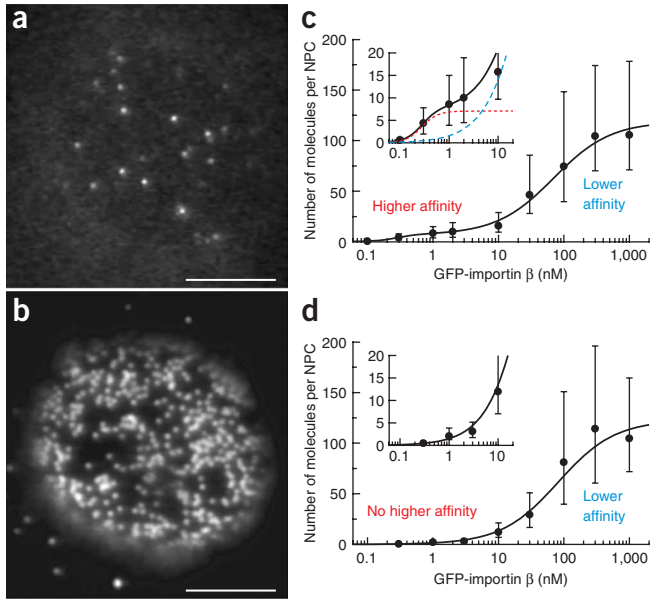

Figure 3 | Visualization of single GFP–importin β molecules and nuclear pores, and a kinetic analysis of the interactions. (**a**) Fluorescence image of single GFP–importin β molecules mediating the cargo transport at the bottom surface of a nucleus (**Supplementary Video 2**). (**b**) NPCs on the bottom of a nucleus. Scale bars, 5 μm. (**c**,**d**) The number of molecules bound to a single NPC, quantified as the ratio of the fluorescence intensities against that of single molecules. (**c**) Binding of cargo-free importin β with the NPC in the absence of Ran and energy sources as a function of the importin β concentration in the incubation medium. Inset, an enlarged graph near the origin. Best fitting gave a sum of two binding functions (solid line), thus indicating that the interaction was composed of two types of binding, namely a higher-affinity binding (dotted red line) and lower-affinity binding (broken blue line). Error bars indicate s.d.; $n = 213$, 134, 273, 286, 235, 254, 128, 139 and 122 NPCs for GFP–importin β = 0.1, 0.3, 1, 2, 10, 30, 100, 300 and 1,000 nM, respectively. (**d**) Binding of the number of cargo (IBB)-bound importin β with the NPC in the absence of Ran and energy sources. Note that higher affinity binding disappeared. Error bars indicate s.d.; $n = 139$, 239, 254, 364, 268, 327, 207 and 258 NPCs for GFP–importin β = 0.3, 1, 3, 10, 30, 100, 300 and 1,000 nM, respectively.

the ratio of signal to background up to 2.2–2.9-fold (**Fig. 2e** and **Supplementary Fig. 3f**). This value is slightly greater than that observed earlier by narrow-field epifluorescence microscopy[14], which is a method to obtain images with a high signal/noise ratio using a pinhole. As a result, HILO illumination microscopy notably increased signal/background ratio up to 7.6-fold (**Fig. 2e**).

We applied this high ratio of signal to background by HILO to single-molecule imaging of nuclear transport inside cells. We visualized single molecules of GFP-importin β mediating the import of cargo through nuclear pores in permeabilized cells as bright spots on the bottom surface of a nucleus (**Fig. 3a** and **Supplementary Video 2** online) at cellular concentrations in or below the nanomolar range. The time course of the fluorescence intensity at the same point showed a one-step appearance and disappearance, a feature of single-molecule images. A single peak in the distribution of fluorescence intensities as well as the mean fluorescence intensity of the spots provided additional evidence that we observed single molecules (**Supplementary Fig. 4** online).

To show effective single-molecule imaging in living cells by HILO, we observed nuclear transport after microinjection of GFP-importin β (**Supplementary Video 3** online). We visualized a glass microneedle by brightfield microscopy illumination with a very small numerical aperture (NA), for easy positioning directly over any target cells. Then we microinjected GFP-importin β into the cytoplasm while monitoring fluorescence images. We observed bright spots with a one-step appearance and disappearance representing single molecules interacting with the NPC during nuclear import. Thus, HILO yields clear single-molecule images in living cells. This high image quality allows the observer to decrease the intensity of the illumination beam.

Next we performed quantitative analysis to demonstrate the application to kinetic studies. At greater than nanomolar concentrations of GFP-importin β in the cell, we clearly visualized individual NPCs as fluorescent spots (**Figs. 1c**, **3b** and **Supplementary Fig. 5a**,**b** online). We evaluated the number of GFP-importin β molecules bound to a single NPC as the ratio of the fluorescence intensities of single NPC images against that of single-molecule images. We distinguished images of a single NPC from two adjoining NPCs by correlation analysis between the fluorescence intensity and the shape of NPC spots (**Supplementary Methods** and **Supplementary Fig. 5**). We obtained the number of bound molecules as a function of the GFP-importin β concentration (**Fig. 3c**,**d**). Importin β in the absence of Ran-GTP exhibited two types of binding with the NPC. The higher affinity binding showed a dissociation constant of 0.3 +0.2/–0.1 nM and a maximum number of bound molecules of 7 +6/–4 molecules/NPC. Its actual number is probably 8 molecules/NPC as the NPC exhibits an eightfold symmetry. The lower affinity binding exhibited almost the same kinetic parameters irrespective of the presence or absence of cargo, with a dissociation constant of 70 +50/−30 nM and a maximum bound number of 110 +60/−40 molecules/NPC. The dissociation constant of isolated nucleoporins with importin β has been reported as ∼100 nM and 0.4–1 nM (ref. 15), which is close to our results.

Here we demonstrated that clear visualization of single molecules in cells enabled the quantification of molecular dynamics, interactions and kinetics. The combined use of *in silico* reconstructions of cell functions with single-molecule quantification will open up new frontiers for life sciences.

Note: Supplementary information is available on the Nature Methods website.

ACKNOWLEDGMENTS

We thank K. Shinkura and K. Takada for assistance, M. Hiroshima, S. Kose, Y. Ue and K. Ebe for technical help, S. Goto and K. Kinosita, Jr. for discussions, and R. Triendl and C. Rowthorn for critical reading of the manuscript. This work was supported by Dynamic Biology Project of New Energy and Industrial Technology Development Organization (M.T.), the Toray Science Foundation (M.T.), Grants-in-Aid from the Ministry of Education, Culture, Sports, Science and Technology of Japan (MEXT) (M.T., N.I., K.S.-S.), and the Advanced and Innovational Research Program of MEXT (M.T.).

AUTHOR CONTRIBUTIONS

M.T. devised and performed microscopy, analysis, kinetics studies and all experiments except biological specimen preparation, and wrote the paper; N.I. contributed biological materials and designed transport experiments; K.S.-S. contributed to image analysis, 3D experiments and 3D microscopy.

Published online at http://www.nature.com/naturemethods/
Reprints and permissions information is available online at http://npg.nature.com/reprintsandpermissions

1. Yanagida, T. *et al. Phil. Trans. R. Soc. Lond. B* **355**, 441–447 (2000).
2. Kinosita, K. Jr., Yasuda, R., Noji, H. & Adachi, K. *Phil. Trans. R. Soc. Lond. B* **355**, 473–489 (2000).
3. Weiss, S. *Nat. Struct. Biol.* **7**, 724–729 (2000).
4. Funatsu, T., Harada, Y., Tokunaga, M., Saito, K. & Yanagida, T. *Nature* **374**, 555–559 (1995).
5. Sase, I., Miyata, H., Corrie, J.E.T., Craik, J.S. & Kinosita, K. Jr. *Biophys. J.* **69**, 323–328 (1995).
6. Tokunaga, M., Kitamura, K., Saito, K., Iwane, A.H. & Yanagida, T. *Biochem. Biophys. Res. Commun.* **235**, 47–53 (1997).
7. Kues, T., Peters, R. & Kubitscheck, U. *Biophys. J.* **80**, 2954–2967 (2001).
8. Yang, W., Gelles, J. & Musser, S.M. *Proc. Natl. Acad. Sci. USA* **101**, 12887–12892 (2004).
9. Kubitscheck, U. *et al. J. Cell Biol.* **168**, 233–243 (2005).
10. Axelrod, D. *J. Cell Biol.* **89**, 141–145 (1981).
11. Kitamura, K., Tokunaga, M., Iwane, A.H. & Yanagida, T. *Nature* **397**, 129–134 (1999).
12. Sako, Y., Minoghchi, S. & Yanagida, T. *Nat. Cell Biol.* **2**, 168–172 (2000).
13. Iino, R., Koyama, I. & Kusumi, A. *Biophys. J.* **80**, 2667–2677 (2001).
14. Yang, W. & Musser, S.M. *Methods* **39**, 316–318 (2006).
15. Pyhtila, B. & Rexach, M. *J. Biol. Chem.* **278**, 42699–42709 (2003).